Impact of Alkali Ions Codoping on Magnetic Properties of $La_{0.9}A_{0.1}Mn_{0.9}Co_{0.1}O_3$ (A: Li, K, Na) Powders and Ceramics

Paweł Głuchowski [1,2,*], Ruslan Nikonkov [1], Robert Tomala [2], Wiesław Stręk [2], Tatsiana Shulha [3], Maria Serdechnova [3], Aleksej Zarkov [4], Tomas Murauskas [4], Andrius Pakalaniškis [4], Ramūnas Skaudžius [4], Aivaras Kareiva [4], Andrei Kholkin [5,6], Maxim Bushinsky [7], Sergei Latushka [7] and Dmitry Karpinsky [7,8]

1   Nanoceramics Inc., Okolna 2, PL-50422 Wroclaw, Poland; r.nikonkov@nanoceramics.pl
2   Institute of Low Temperature and Structural Research PAS, Okolna 2, PL-50422 Wroclaw, Poland; r.tomala@intibs.pl (R.T.); w.strek@intibs.pl (W.S.)
3   Helmholtz-Zentrum Geesthacht, Zentrum für Material- und Küstenforschung GmbH, Max-Planck-Straße 1, DE-21502 Geesthacht, Germany; Tatsiana.Shulha@hzg.de (T.S.); Maria.Serdechnova@hzg.de (M.S.)
4   Department of Inorganic Chemistry, Vilnius University, Universiteto g. 3, LT-01513 Vilnius, Lithuania; a.zharkoff@gmail.com (A.Z.); tomas.murauskas@chf.vu.lt (T.M.); pakalniskis.andrius@gmail.com (A.P.); ramunas.skaudzius@chgf.vu.lt (R.S.); aivaras.kareiva@chgf.vu.lt (A.K.)
5   School of Natural Sciences and Mathematics, Ural Federal University, Kuybysheva 48, RU-620026 Ekaterinburg, Russia; kholkin@ua.pt
6   CICECO-Materials Institute of Aveiro and Physics Dept, University of Aveiro, PT-3810-193 Aveiro, Portugal
7   Scientific and Practical Materials Research Center NAS Belarus, P. Brovki 19, BY-220072 Minsk, Belarus; bushinsky@physics.by (M.B.); smer444@mail.ru (S.L.); dmitry.karpinsky@gmail.com (D.K.)
8   Nanotechnology Research & Education Centre, South Ural State University, Lenin av., 76, RU-454080 Chelyabinsk, Russia
*   Correspondence: p.gluchowski@nanoceramics.pl or p.gluchowski@intibs.pl

Abstract: The aim of the work was to check how the introduction of alkali and cobalt ions into a manganese structure can affect the structural disorder and, in consequence, lead to the changes (improvements) of magnetic properties. The high-pressure sintering technique was applied to check if the external factor can modify the magnetization of manganites. Nanocrystalline $La_{0.9}A_{0.1}Mn_{0.9}Co_{0.1}O_3$ (where A is Li, K, Na) powders were synthesized by the combustion technique. The respective powders were used for nanoceramics preparation by the high-pressure sintering technique. The structure and morphology of the compounds were studied by X-ray powder diffraction, scanning electron microscopy and energy-dispersive X-ray spectroscopy. Magnetization studies for all compounds were performed in order to check the changes induced by either codoping or the sintering pressure. It was found that the type of the dopant ion and sintering pressure produced significant changes to the magnetic properties of the studied compounds. Alkali ions lead to the stabilization of Co ions in the +2 oxidation state and the formation of positive exchange interactions Mn^{3+}–Mn^{4+} and Co^{2+}–Mn^{4+} and the subsequent increase in remanent magnetization. High sintering pressure leads to a decrease in grain size and reduction of long-range ferromagnetic order and lower magnetization.

Keywords: multiferroic; manganites; alkaline ions; transition metal ions; nanoceramics; magnetization

1. Introduction

Multiferroics are compounds which in one phase exhibit more than one primary ferroic order (ferromagnetism, ferroelectricity or ferroelasticity) [1]; however, in recent years this term has been

mainly used for magnetoelectric materials. Such materials have both magnetic and ferroelectric properties simultaneously. To obtain magnetic materials where magnetic moments are not cancelled out by each other, it is necessary to exclude all ions where outer orbitals are completely filled. This limits the potential multiferroic materials to systems containing either transition metals with partially filled 3d shells or lanthanides with partially filled 4f shells. In the case of ferroelectricity, the Jahn–Teller effect has to be taken into account [2], where oppositely charged ions form a local dipole with a spatially degenerate electronic ground state. For the purpose of removing this degeneracy in the structure, a geometrical distortion appears to lead to the lowering of the overall energy of the system. The mentioned effect and the character of the chemical bonds favor ferroelectricity in such systems. The research conducted in the last two decades showed that the nature of colossal magnetoresistance effect (CMR) [3–9] in lanthanum manganates cannot be explained without invoking the mechanism of the Jahn–Teller distortion of MnO_6 octahedra. The effect of distortions on magnetic interactions and electron transfer can be induced by structural stresses which are lessened by MnO_6 array oxidation and by the doping the structure by ions with different ionic radii [10–12].

The combination and control of simultaneous ferroic orderings is still a challenge for scientists all around the world. The studies are conducted mainly towards the development of new materials in which, by changing their chemical composition, morphology or form, it will be possible to intentionally introduce the desired properties. The possibility of designing unique magnetic properties and coexistence of Mn^{3+} and Mn^{4+} ions allows for the widening of the range of applications for lanthanum manganates and lanthanum manganates doped with transition metal ions in $Li-O_2$ batteries [6], solid oxide fuel cells [13–15], alkaline fuel cells [16], magnetic refrigeration [17], and catalysts in oxidation reaction [8,18,19].

Cobalt doped lanthanum manganite attracts a great deal of attention as catalytic material. The bifunctional catalytic activity of oxygen reduction reaction (ORR) and oxygen evolution reaction (OER) can be tailored by the substitution of manganese ions by cobalt ions and control the Mn^{3+}/Mn^{4+} ratio [8,9]. The chemical doping of manganese ions by cobalt ions as well as diamagnetic A-site substitution with alkali elements can be used as an effective tool to control the magnetic properties of the $LaMnO_3$-based compounds [7,20]. The Curie temperature, below which material exhibits ferromagnetic properties, is the highest when the concentration of Mn^{4+} is in the range of 25–30% [20,21]. It was reported that point defects, dependent on the oxygen content, strongly influenced the physical properties of manganites [5,8]. One of the possible ways of inducing defects to the matrix is aliovalent doping which leads also to the oxidation of Mn-array [5,22]. Kim et al. observed that the effect can also tune the electrochemical polarization leading to the dopant segregation in the matrix [23].

This work proposes a new approach to changing the magnetic properties of one of the types of manganites by introducing aliovalent ions and applying pressure. The paper is a continuation of our work on changing the magnetic properties of manganites by doping their structure with alkaline metal ions [24].

2. Materials and Methods

To obtain the $La_{0.9}A_{0.1}Mn_{0.9}Co_{0.1}O_3$ (where A is Li, K, Na) compounds, the combustion method was applied [25]. Firstly, lanthanum (REacton®, 99.999%, Karlsruhe, Germany), manganese (Puratronic®, 99.995%, Karlsruhe, Germany) and cobalt (ACS, 98.0–102.0%, Washington, DC, USA) nitrates, and A–precursors ($LiNO_3$-ACS, 99.0% min, $NaNO_3$-ACS, 99.0% min or KNO_3 ACS, 99.0% min, Washington, DC, USA) with the molar ratio of La/A and Mn/Co = 0.9/0.1 were dissolved in distilled water. Then 10% of molten stearic acid (Calbiochem, San Diego, CA, USA) was added to the solution in a porcelain reactor. The resulting mixture was continuously stirred and kept at a temperature of 140 °C. After 2 h La-Mn-stearic acid formed a gel. Then, the porcelain crucible reactor was placed in a furnace and heated up to 500 °C. The gel volatilized and auto ignited; with the evolution of a large volume of gases it produced loose grey powder. The obtained powders were ground in the agate mortar and additionally calcined at 700 °C for 1 h to remove all organic residues. After calcination, all powders

were grinded and taken for further experiments. Half of the powders were used for ceramics sintering, using the high pressure sintering technique [26]. For a short duration powders were pressed (200 MPa) at room temperature to "green body" (GB). The GB was placed into a $CaCO_3$ container with a graphite heater and the inside was isolated by hexagonal boron nitride. The shape of the container allowed to keep isostatic pressure during axial pressing. After the application of 8 GPa pressure, the pellets were sintered at 500 °C for 1 min into ceramics. After sintering, the as obtained ceramics were polished and taken for further studies.

The structure of the powders and ceramics were characterized and analyzed by powder X-ray diffraction (XRD) using a PANalytical X'Pert diffractometer (Malvern Panalytical, Almelo, The Netherlands) with Ni-filtered CuK_λ radiation, $\lambda = 1.5418$ Å with the step of 0.02626 2θ for 1 h. The powders and ceramics were measured in the reflection mode. In the case of the powder, it was ground and placed directly in the sample holder, while the ceramics were placed in plasticine so that the surface of the ceramics would be parallel to the surface of the holder. For SEM imaging, the powders were ground in an agate mortar and glued to the carbon tape. The excess powder was removed using compressed air and the prepared material was taken for measurements. In the case of ceramics, the sample was simply glued to the carbon tape on the holder. Scanning electron microscopy (SEM) characterization was conducted using a commercial Tescan Vega3 SB microscope (SEM, Brno, Czech Republic) at 5 kV (acceleration voltage) with 3.5 spot (size of electron beam) and 3.2–3.7 mm working distance in order to analyze grain size and morphology. The chemical homogeneity of the powders and ceramics was measured using a scanning electron microscope FESEM FEI Nova NanoSEM 230 equipped with an energy dispersive spectroscopy (EDS) spectrometer (EDAX Genesis) at 18 kV (acceleration voltage) with 4.0 spot (size of electron beam) and 4.0 mm working distance. The XPS analysis was carried out with a Kratos Axis Supra spectrometer using monochromatic Al K(alpha) source (25 mA, 15 kV). The instrument work function was calibrated to give the binding energy (BE) of 83.96 eV for the Au 4f7/2 line for metallic gold, and the spectrometer dispersion was adjusted to give a BE of 932.62 eV for the Cu 2p3/2 line of metallic copper. The Kratos charge neutralizer system was used on all specimens. Survey scan analyses were carried out with an analysis area of 300×700 microns and a pass energy of 160 eV. High resolution analyses were carried out with an analysis area of 300×700 microns and a pass energy of 20 eV. The spectra were charge corrected to the main line of the carbon 1s spectrum (adventitious carbon) set to 284.8 eV. The spectra were analyzed using the CasaXPS software (version 2.3.23rev11.1R). The magnetic properties of the powders and ceramics were evaluated, using the Physical Properties Measurement Systems from Cryogenic Ltd. (London, UK) in magnetic fields up to ±14 T at 5 K.

3. Results

3.1. Structure and Morphology

The $La_{0.9}A_{0.1}Mn_{0.9}Co_{0.1}O_3$ powders and ceramics were characterized by X-ray diffraction at room temperature (Figure 1). The crystal structure and the unit cell parameters were calculated using the Rietveld refinement with the X'pert HighScore Plus software using the pseudo-Voigt profile shape function, the background profile was fitted by the Lagrangian polynomial of 5th order [27]. This procedure allowed to attest the phase purity of the compounds and also to determine the crystal structure and structural parameters. The analysis of the XRD results indicated the rhombohedral symmetry described by *R-3c* space group (ICSD 75070) [28], which are similar to the structural results obtained for the $La_{0.9}A_{0.1}MnO_3$ compounds, previously studied by the authors [24], and other $LaMnO_3$-based compounds [29]. It should be noted that the crystal structure of undoped compounds is also characterized by the rhombohedral distortion of the unit cell which implies nominal oxygen excess in $LaMnO_{3+\delta}$ ($\delta > 1\%$) compounds [30], leading to nonzero remanent magnetization as compared to stoichiometric $LaMnO_3$ having an orthorhombic structure [31].
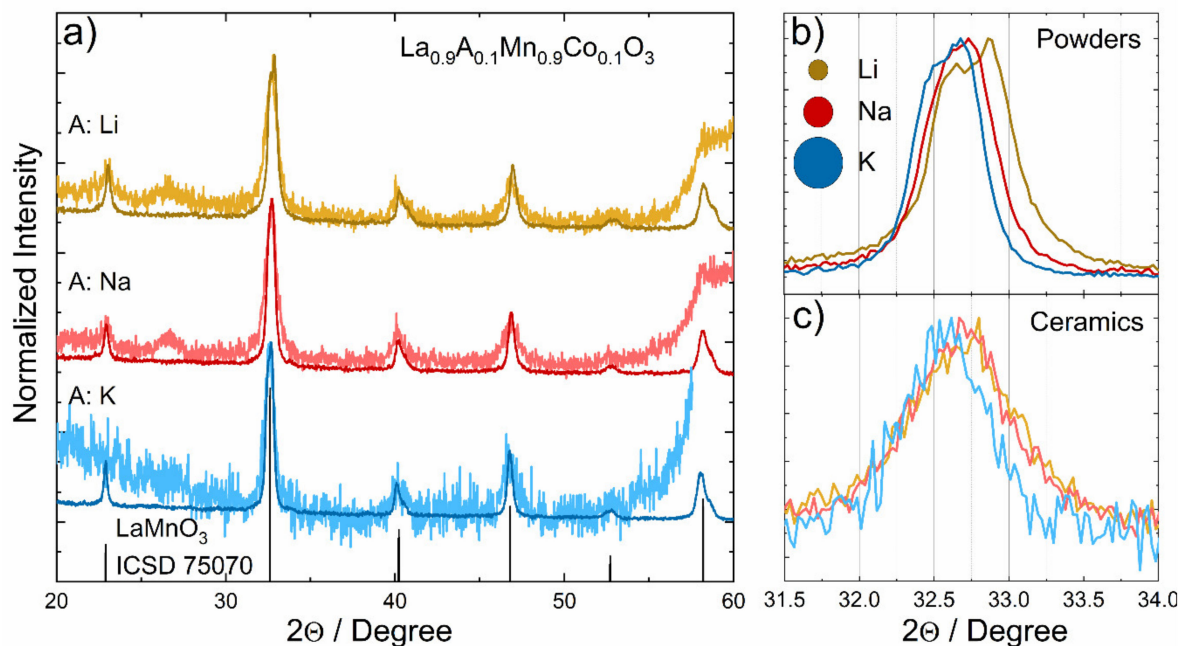
Figure 1. XRD patterns recorded for $La_{0.9}A_{0.1}Mn_{0.9}Co_{0.1}O_3$ powders and ceramics (**a**). The right panel shows enlarged region of the pattern, with shift of the peak and with change of the dopant ionic radius observed in powders (**b**) and broadening of the peak observed for ceramics (**c**).

After the application of pressure, the diffraction peaks became wider, which may indicate a decrease in grain size associated with the decomposition of particle shells from the crystalline to amorphous state, such a phenomenon has already been described in our previous study [32]. In addition, the broadening of reflections is associated with the introduction of additional strains into the structure induced by high pressure during the sintering process [33]. It should be noted that the introduction of the bigger ion and the pressure applied during sintering lead to an increase in the strain in the compounds. It was observed that the introduction of 10 mol.% of alkali ions does not change the structure but clearly shifts the peaks to the higher 2θ degrees and increases the ionic radii [34]. This suggests an expansion of the unit cells and an increase in their volumes (Table 1) as confirmed by the results of the Rietveld refinement analysis. It should be noted that no additional peaks coming from the secondary phase were observed for the initial powder compounds, while the XRD patterns of the ceramic compounds contain distinct extra reflection located at ~26.5 2θ deg. The observed reflection is attributed to h-BN material integrated into tablets during the pressure procedure, which does not affect the crystal structure and the magnetic properties. In the case of ceramics, the applied pressure leads to a decrease in the unit cell volume, which has a significant impact on the magnetic properties of the ceramics as compared to the starting powders [35]. As the XRD measurements were performed in the reflection mode, the ceramics are small and, in some cases, they do not have parallel surfaces, the XRD patterns at high 2Θ degrees become noisy and the baseline rises. However, the main peak observed at lower degrees shows that the structure of the ceramics remains unchanged and is described by the rhombohedral symmetry.

Table 1. Average crystallite size and the cell parameters calculated for $La_{0.9}A_{0.1}Mn_{0.9}M_{0.1}O_3$ powders and ceramics based on the XRD data.

	Crystallite Size	a, b	c	V	Strain
	nm	Å	Å	Å³	%
Powders					
$La_{0.9}Li_{0.1}Mn_{0.9}Co_{0.1}O_3$ R_{wp} = 2.897; R_{exp} = 1.991; GOF = 2.119	22	5.5073(3)	13.3145(3)	349.73(4) (58.29)	0.008
$La_{0.9}Na_{0.1}Mn_{0.9}Co_{0.1}O_3$ R_{wp} = 3.216; R_{exp} = 1.993; GOF = 3.113	26	5.5041(1)	13.3375(4)	349.92(9) (58.32)	0.045
$La_{0.9}K_{0.1}Mn_{0.9}Co_{0.1}O_3$ R_{wp} = 4.285; R_{exp} = 2.012; GOF = 4.899	33	5.5127(1)	13.3567(3)	351.52(8) (58.59)	0.054
Ceramics					
$La_{0.9}Li_{0.1}Mn_{0.9}Co_{0.1}O_3$ R_{wp} = 11.004; R_{exp} = 8.322; GOF = 9.849	9	5.5060(8)	13.3123(7)	348.64(3) (58.11)	0.063
$La_{0.9}Na_{0.1}Mn_{0.9}Co_{0.1}O_3$ R_{wp} = 13.415; R_{exp} = 9.071; GOF = 10.185	11	5.5080(3)	13.3198(7)	349.47(6) (58.25)	0.065
$La_{0.9}K_{0.1}Mn_{0.9}Co_{0.1}O_3$ R_{wp} = 17.080; R_{exp} = 12.096; GOF = 14.003	12	5.5058(7)	13.3755(8)	351.15(2) (58.55)	0.077

R_{wp}—Weighted Profile Rietveld R-factor, R_{exp}—Expected Rietveld R-factor, GOF—goodness of fit.

The SEM images show that the combustion synthesis significantly affects grain morphology (Figure 2). Short synthesis time allows one to obtain nanosized crystallites and later calcination leads to their agglomeration. The high temperature generated during self-combustion (above 1500 °C) and relatively short calcination time causes broad grain size distribution and the crystallization of bigger grains [36]. However, even after the calcination of the powder for one hour, it can be seen that bigger aggregates are composed of smaller grains.

For powders and ceramics codoped with different alkali ions, the energy dispersive spectroscopy (EDS) maps were prepared to check the elements distribution and confirm that there is no segregation of particular ions on grain boundaries (Figure 3). The EDS analysis reveals that the concentration of the sodium and potassium is 10 mol% of La, as was assumed at the preparation stage, also cobalt ions substitute about 10% of manganese ions. For the powders and ceramics codoped with lithium, it was impossible to register signal from the dopant alkali ions as these ions are too light to be reliably registered by the analyzer. It can also be concluded that oxygen content in ceramics is about 10% lower than in powders, which was also confirmed in the EDS maps (Figure 3). It should be noted that the assessment of oxygen content by the EDS method has a rather qualitative character; however, at the same time the obtained results can allow one to estimate the evolution in the oxygen content as a function of the dopant ions and to determine a difference in the oxygen content in powder and ceramic samples.
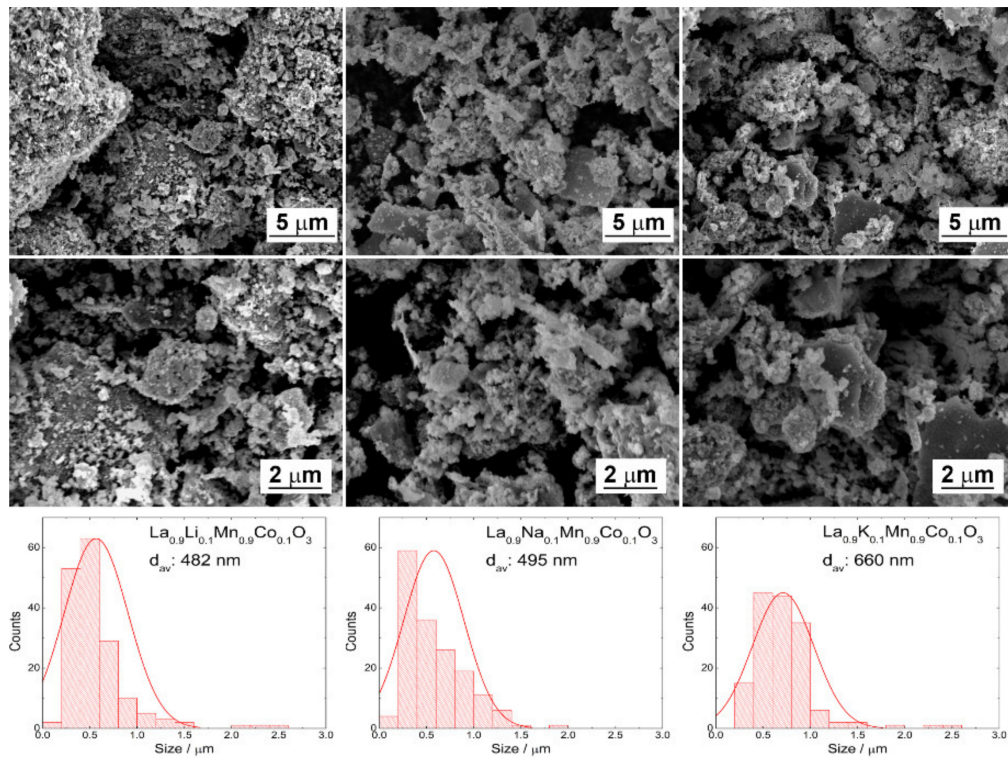
Figure 2. SEM images and particle size distribution of $La_{0.9}A_{0.1}Mn_{0.9}Co_{0.1}O_3$ (A: Li, Na, K) powders.
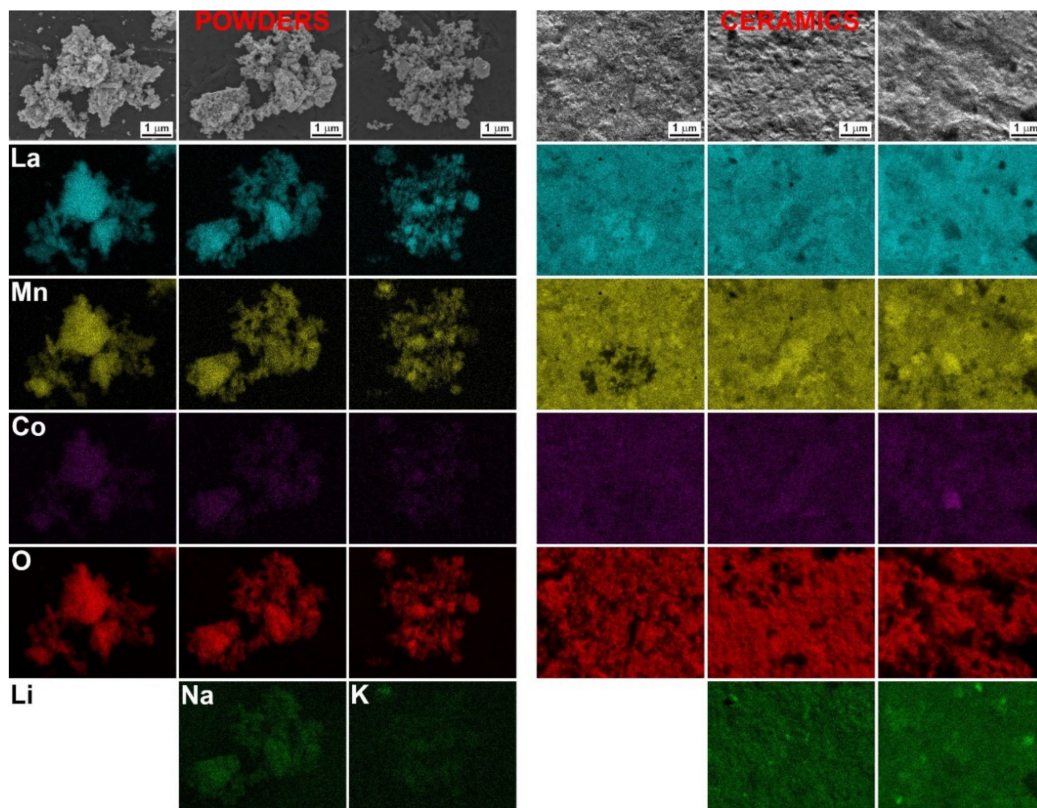

Figure 3. Energy dispersive spectroscopy (EDS) maps of $La_{0.9}A_{0.1}Mn_{0.9}Co_{0.1}O_3$ powders (**left**) and ceramics (**right**).

3.2. Determination of Oxidation States of Mn and Co Ions

The high-resolution Mn 2p and Co 2p XPS spectra of $La_{0.9}A_{0.1}Mn_{0.9}Co_{0.1}O_3$ (A: Li, K, Na) ceramics are shown in Figure 4. It can be seen that the Mn 2p spectrum consists of two asymmetric peaks located at 641.8 (Mn $2p_{3/2}$) and 653.3 eV (Mn $2p_{1/2}$). Both of these peaks can be deconvoluted into two peaks centered at 641.5 and 643.1 eV, and at 653.1 and 654.3 eV, respectively. The peaks located at 641.5 and 653.1 eV correspond to Mn^{3+} ions, while the peaks located at 643.1 and 654.3 eV are assigned to Mn^{4+} ions [37–39]. The absence of a satellite peak at +5 eV from Mn $2p_{3/2}$ indicates that no Mn^{2+} is present [40]. The Co 2p XPS spectrum exhibited two main peaks, corresponding to the $2p_{3/2}$ and $2p_{1/2}$ levels, and shake-up satellite peaks centered at around 790.0 and 796.9 eV. Similarly as in the case of Mn, the asymmetric peaks of Co $2p_{1/2}$ and Co $2p_{3/2}$ can be resolved into components. The results indicate that Co ions exist in the Co^{2+} and Co^{3+} oxidation state. The peaks at lower BE were attributed to Co^{3+} oxidation state, whereas the peaks at higher BE to Co^{2+} [41]. The atomic ratio of Mn^{3+}/Mn^{4+} and Co^{2+}/Co^{3+} is summarized in Table 2.
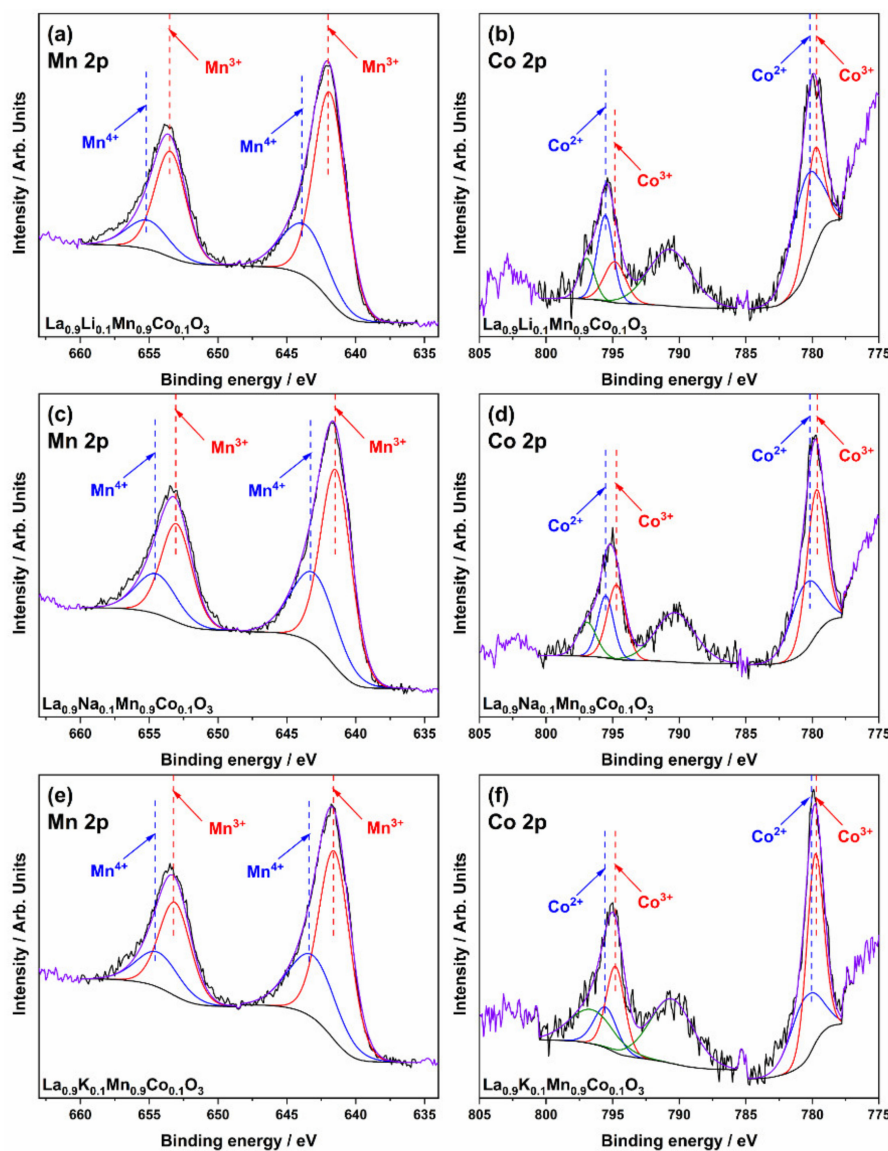
Figure 4. Mn 2p and Co 2p XPS spectra of $La_{0.9}Li_{0.1}Mn_{0.9}Co_{0.1}O_3$ (**a,b**), $La_{0.9}Na_{0.1}Mn_{0.9}Co_{0.1}O_3$ (**c,d**) $La_{0.9}K_{0.1}Mn_{0.9}Co_{0.1}O_3$ (**e,f**) ceramics.

Table 2. Oxidation state of Mn and Co ions in synthesized powders and ceramics.

	Mn Oxidation State (%)		Co Oxidation State (%)	
	3+	4+	2+	3+
Powders				
$La_{0.9}Li_{0.1}Mn_{0.9}Co_{0.1}O_3$	73.2	26.8	61.1	38.9
$La_{0.9}Na_{0.1}Mn_{0.9}Co_{0.1}O_3$	75.2	24.8	42.9	57.1
$La_{0.9}K_{0.1}Mn_{0.9}Co_{0.1}O_3$	67.2	32.8	39.9	60.1
Ceramics				
$La_{0.9}Li_{0.1}Mn_{0.9}Co_{0.1}O_3$	75.8	24.2	60.2	39.8
$La_{0.9}Na_{0.1}Mn_{0.9}Co_{0.1}O_3$	65.1	34.9	41.7	58.3
$La_{0.9}K_{0.1}Mn_{0.9}Co_{0.1}O_3$	66.3	33.7	37.0	63.0

3.3. Magnetic Properties

The results of magnetization measurements clarified the modifications which occurred in the magnetic structure of lanthanum manganates driven by chemical codoping by alkali elements and cobalt ions (Figure 5). The results of magnetization measurements obtained for the undoped compound indicate the inhomogeneous magnetic state with a strong ferromagnetic component which is observed for the compounds regardless the preparation procedure. The complex magnetic structure of the initial $LaMnO_3$ compound is associated with a lack in the cation content and thus the nominal excess of oxygen content leading to the formation of competing positive (Mn^{3+}–O–Mn^{4+}) and negative (Mn^{3+}–O–Mn^{3+}; Mn^{4+}–O–Mn^{4+}) exchange interactions associated with ferromagnetic and antiferromagnetic orders, respectively. The competing antiferromagnetic and ferromagnetic phases lead to the formation of a mixed magnetic state, which is characteristic for $LnMnO_3$-based systems [24,42–45]. Chemical substitution with alkali elements and cobalt ions leads to an increase in the magnetization of the compounds which is caused by the higher number of manganese ions having +4 oxidation state and thus leading to the strengthening of positive exchange interactions Mn^{3+}–Mn^{4+}. Certain deviations from the above mentioned tendency were ascribed to the modification in the oxidation during the synthesis process [24] and thus to variations in the exchange interactions formed between Co and Mn ions.

The powder samples codoped with sodium and cobalt ions possess the maximal value of magnetization among the compounds of both series. The difference in the magnetization at the magnetic field of 14 T of the doped compound as compared to the initial $LaMnO_3$ is about 30% (Figure 5). The observed increase in magnetization is most probably associated with the increase in the amount of Mn^{4+} ions and the stabilization of Co ions in +2 oxidation state. The rise in the amount of Mn^{4+} strengthens ferromagnetism in the compounds, due to positive exchange interactions Mn^{3+}–Mn^{4+}. Simultaneously, the presence of Co^{2+} ions causes the formation of new positive interactions Co^{2+}–Mn^{4+}. The stabilization of the cobalt ions in +2 oxidation state is in accordance with the notable increase in magnetic anisotropy observed for the doped compound ($H_C \sim 0.2$ T for the compound $La_{0.9}Li_{0.1}Mn_{0.9}Co_{0.1}O_3$ as compared to $H_C \sim 0.02$ T of the initial compound). It should be noted that the ionic radius of the Co^{2+} ions (0.53Å for ion in high spin state and octahedral coordination) nearly coincides with the radius of Mn^{4+} ions with the same coordination, which facilitates the occupation of *B*- position of the perovskite lattice. The stabilization of +2 oxidation state of the cobalt ions is also in accordance with the structural data showing a gradual increase in the unit cell volume with chemical doping. One can conclude about the optimal concentration of the amount of Mn^{3+} and Mn^{4+} ions in the compounds codoped with sodium (potassium) and cobalt ions which show maximal magnetization due to the dominance of strongly positive exchange interactions Mn^{3+}–Mn^{4+}.
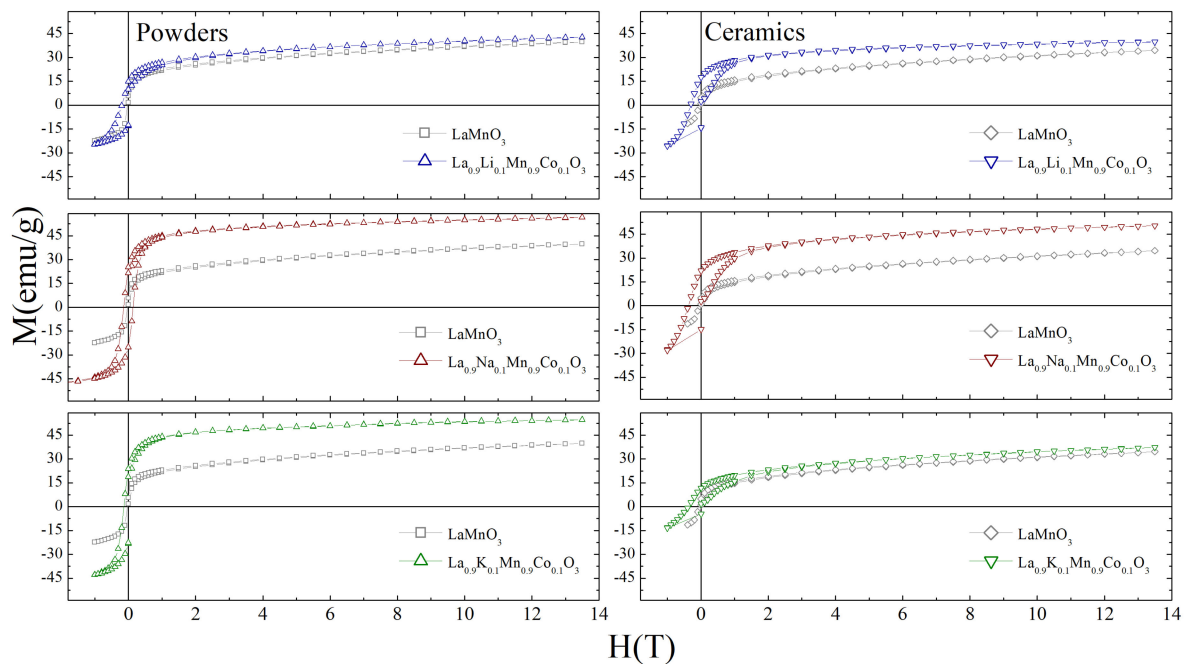
Figure 5. Isothermal magnetization curves measured for the initial $LaMnO_3$ and codoped $La_{0.9}A_{0.1}Mn_{0.9}Co_{0.1}O_3$ (A: Li, Na, K) powders (**left**) and ceramics (**right**) at T = 5 K (the graphs presented using the same scales).

It should be noted that the magnitude of magnetization observed for the compound codoped with Li and Co ions is notably lower than the magnetization observed for other doped compounds in the powder form. The coercivity of the compound codoped with Li and Co ions is about 40% larger than the values observed for other doped compounds, which indicates a larger amount of the cobalt ions in +2 oxidation state as confirmed by XPS measurements. Examining isothermal magnetization dependences, one can assume that the magnetic state of the Li- and Co- codoped compounds is determined by the coexistence of positive exchange interactions formed between Co^{2+}–Mn^{4+} ions and negative interactions Mn^{3+}–Mn^{3+} and Co^{2+}–Mn^{3+}.

The ceramic compounds are characterized by a lower value of magnetization as compared to the related powder samples, which is caused by a reduced amount of oxygen content occurring during the high pressure procedure, as indirectly confirmed by the EDS and XPS data. The smaller amount of oxygen content results in the increase in the number of structural defects, which frustrates exchange interactions thus leading to the mixed magnetic state. As in the case of the compounds in the powder form, chemical doping leads to the stabilization of +2 oxidation state of the cobalt ions, which leads to an increase in the value of coercivity. The stabilization of cobalt ions in +2 oxidation state leads to an increase in the magnetization of the compounds doped with sodium (lithium) and cobalt ions, which can be caused by the formation of positive exchange interactions Co^{2+}–Mn^{4+} ions. Magnetization estimated for the potassium and cobalt codoped compound is notably lower in comparison to the other codoped compounds, especially in the low field region, which can be explained by a more distinct reduction in oxygen content that occurred in these compounds during the high pressure procedure. The deficit in the oxygen content frustrates the dominant long-range ferromagnetic order, thus reducing spontaneous magnetization; moreover, an increase in the amount of oxygen vacancies provides negative Mn^{3+}–Mn^{3+} and Co^{2+}–Mn^{3+} interactions and thus fosters the stabilization of the mixed magnetic state characteristic of the initial $LaMnO_3$ compound (Figure 5). The nonsystematic evolution of magnetization observed for the ceramic compounds can be explained by the absorption of oxygen by a sample holder during high pressure treatment. The formation of nanoscale crystallites with an average size of a few tens of nanometers, due to the application of high pressure, causes

a reduction in magnetization for all ceramic compounds as compared to powders because of the disturbance of the long range magnetic order associated with ferromagnetism.

4. Discussion and Conclusions

The combustion method may be applied for fast and effective manganese powders production, also with a different type of codopants. The analysis of the structure and morphology of the manganites doped with cobalt ions and codoped with alkali ions shows the expansion of the unit cell with an increase in the alkali metal ion radius. It does not have an impact on the crystallization in the proper structure although it shows a great influence on the magnetic properties of the powders. It may also be concluded that applying high pressure during the sintering leads to a decrease in grains size, amorphization of grain shells and changes in the magnetic properties of the ceramics. The results of magnetization measurements point at the mixed magnetic state of the undoped compounds $LaMnO_3$, regardless of the preparation procedure which is caused by the nominal excess of oxygen content and thus the formation of competing positive Mn^{3+}–O–Mn^{4+} exchange interactions and negative Mn^{3+}–O–Mn^{3+}; Mn^{4+}–O–Mn^{4+} interactions. Chemical doping with alkali and cobalt ions leads to the stabilization of Co ions in +2 oxidation state thus leading to the formation of positive Mn^{3+}–Mn^{4+} and Co^{2+}–Mn^{4+} exchange interactions and an increase in remanent magnetization. The difference in the magnetization values observed for the compounds in the powder form is caused by a certain deviation in the oxygen content formed during the preparation process. Ceramic compounds are characterized by lower magnetization as compared to the compounds in the powder form having the same chemical compositions, which is caused by a more intense reduction in oxygen content that occurred in the surface layer of the samples near the sample-*h*BN interface in the high pressure matrix and the nanometer size of the crystallites causing a reduction in the long range ferromagnetic order.

Author Contributions: P.G. conceived and planned the experiments and wrote the manuscript with support from other coauthors, R.N. synthesized powders, R.T. prepared ceramics, W.S. supervised the project, T.S. performed SEM/EDS measurements of powders, M.S. analyzed SEM/EDS measurements, T.M. performed XPS measurements, A.Z. analyzed XPS spectra, A.P. synthesized powders, R.S. supervised the synthesis and analyzed structural measurements, A.K. (Aivaras Kareiva) supervised the synthesis and analyzed the results, A.K. (Andrei Kholkin) analyzed and discussed the results, M.B. measured the magnetic properties of powders and ceramics, S.L. XRD data refinement, D.K. analyzed the magnetic properties of powders and ceramics. All authors provided critical feedback and helped shape the research, analysis and manuscript. All authors have read and agreed to the published version of the manuscript.

References

1. Schmid, H. Multi-ferroic magnetoelectrics. *Ferroelectrics* **1994**, *162*, 317–338. [CrossRef]
2. Jahn, H.A.; Teller, E. Stability of polyatomic molecules in degenerate electronic states—I—Orbital degeneracy. *Proc. R. Soc. Lond. Ser. A Math. Phys. Sci.* **1937**, *161*, 220–235. [CrossRef]
3. Rivero, P.; Meunier, V.; Shelton, W. Electronic, structural, and magnetic properties of $LaMnO_3$ phase transition at high temperature. *Phys. Rev. B* **2016**, *93*, 024111. [CrossRef]

4. Norby, P.; Andersen, I.; Andersen, E.; Andersen, N.H. The crystal structure of lanthanum manganate(iii), LaMnO$_3$, at room temperature and at 1273 K under N2. *J. Solid State Chem.* **1995**, *119*, 191–196. [CrossRef]

5. Malavasi, L.; Ritter, C.; Mozzati, M.C.; Tealdi, C.; Islam, M.S.; Azzoni, C.B.; Flor, G. Effects of cation vacancy distribution in doped LaMnO$_3$+δ perovskites. *J. Solid State Chem.* **2005**, *178*, 2042–2049. [CrossRef]

6. Lv, Y.; Li, Z.; Yu, Y.; Yin, J.; Song, K.; Yang, B.; Yuan, L.; Hu, X. Copper/cobalt-doped LaMnO$_3$ perovskite oxide as a bifunctional catalyst for rechargeable Li-O$_2$ batteries. *J. Alloy. Compd.* **2019**, *801*, 19–26. [CrossRef]

7. Liu, X.; Gong, H.; Wang, T.; Guo, H.; Song, L.; Xia, W.; Gao, B.; Jiang, Z.; Feng, L.; He, J. Cobalt-Doped Perovskite-Type Oxide LaMnO$_3$ as Bifunctional Oxygen Catalysts for Hybrid Lithium-Oxygen Batteries. *Chem. Asian J.* **2018**, *13*, 528–535. [CrossRef]

8. Zhu, W.; Chen, X.; Liu, Z.; Liang, C. Insight into the Effect of Cobalt Substitution on the Catalytic Performance of LaMnO$_3$ Perovskites for Total Oxidation of Propane. *J. Phys. Chem. C* **2020**, *124*, 14646–14657. [CrossRef]

9. Flores-Lasluisa, J.X.; Huerta, F.; Cazorla-Amorós, D.; Morallon, E. Structural and morphological alterations induced by cobalt substitution in LaMnO$_3$ perovskites. *J. Colloid Interface Sci.* **2019**, *556*, 658–666. [CrossRef]

10. Krishnan, R.V.; Banerjee, A. Evidence of dynamic Jahn-Teller effects in ferromagnetism of rhombohedral Al-substituted lanthanum manganite. *J. Phys. Condens. Matter* **2000**, *12*, 3835–3847. [CrossRef]

11. Golenishchev-Kutuzov, A.V.; Golenishchev-Kutuzov, V.A.; Kalimullin, R.I.; Semennikov, A.V. Ordered states of Jahn-Teller distorted MnO6 octahedra in weakly doped lanthanum-strontium manganites. *Phys. Solid State* **2015**, *57*, 1633–1638. [CrossRef]

12. Bogdanova, K.G.; Bulatov, A.R.; Golenishchev-Kutuzov, V.A.; Potapov, A.A. Influence of the Jahn-Teller effect on the structural, magnetic, and electrical properties of lightly doped manganites. *Bull. Russ. Acad. Sci. Phys.* **2013**, *77*, 275–277. [CrossRef]

13. shihara, T. *Perovskite Oxide for Solid Oxide Fuel Cells*; Springer: New York, NY, USA, 2009; ISBN 78-0-387-77707-8.

14. Jin, S.; Tiefel, T.H.; McCormack, M.; Fastnacht, R.A.; Ramesh, R.; Chen, L.H. Thousandfold Change in Resistivity in Magnetoresistive La-Ca-Mn-O Films. *Science* **1994**, *264*, 413–415. [CrossRef] [PubMed]

15. Tao, S.; Irvine, J.T.S.; Kilner, J.A. An Efficient Solid Oxide Fuel Cell Based upon Single-Phase Perovskites. *Adv. Mater.* **2005**, *17*, 1734–1737. [CrossRef]

16. Ahmad, E.A.; Mallia, G.; Kramer, D.; Kucernak, A.R.; Harrison, N.M. The stability of LaMnO$_3$ surfaces: A hybrid exchange density functional theory study of an alkaline fuel cell catalyst. *J. Mater. Chem. A* **2013**, *1*, 11152–11162. [CrossRef]

17. Morelli, D.T.; Mance, A.M.; Mantese, J.V.; Micheli, A.L. Magnetocaloric properties of doped lanthanum manganite films. *J. Appl. Phys.* **1996**, *79*, 373–375. [CrossRef]

18. 18. Jia, M.; Li, X.; Zhaorigetu; Shen, Y.; Li, Y. Activity and deactivation behavior of Au/LaMnO$_3$ catalysts for CO oxidation. *J. Rare Earths* **2011**, *29*, 213–216. [CrossRef]

19. Zhang, C.; Guo, Y.; Guo, Y.; Lu, G.; Boreave, A.; Retailleau, L.; Baylet, A.; Giroir-Fendler, A. LaMnO$_3$ perovskite oxides prepared by different methods for catalytic oxidation of toluene. *Appl. Catal. B Environ.* **2014**, *148–149*, 490–498. [CrossRef]

20. Schiffer, P.; Ramirez, A.P.; Bao, W.; Cheong, S.-W. Low Temperature Magnetoresistance and the Magnetic Phase Diagram of La1−xCaxMnO$_3$. *Phys. Rev. Lett.* **1995**, *75*, 3336–3339. [CrossRef]

21. Mahendiran, R.; Tiwary, S.; Raychaudhuri, A.; Ramakrishnan, T.; Mahesh, R.; Rangavittal, N.; Rao, C. Structure, electron-transport properties, and giant magnetoresistance of hole-doped systems. *Phys. Rev. B Condens. Matter Mater. Phys.* **1996**, *53*, 3348–3358. [CrossRef]

22. Bara, M.; Dzik, J.; Feliksik, K.; Kozielski, L.; Wodecka-Duś, B.; Goryczka, T.; Zarycka, A.; Adamczyk-Habrajska, M. Influence of calcium ions on the structure and properties of LaMnO$_3$. *Arch. Metall. Mater.* **2020**, *65*, 1189–1195.

23. Kim, D.; Bliem, R.; Hess, F.; Gallet, J.-J.; Yildiz, B. Electrochemical Polarization Dependence of the Elastic and Electrostatic Driving Forces to Aliovalent Dopant Segregation on LaMnO$_3$. *J. Am. Chem. Soc.* **2020**, *142*, 3548–3563. [CrossRef] [PubMed]

24. Głuchowski, P.; Nikonkov, R.; Tomala, R.; Stręk, W.; Shulha, T.; Serdechnova, M.; Zheludkevich, M.; Pakalaniškis, A.; Skaudžius, R.; Kareiva, A.; et al. Magnetic Properties of La$_{0.9}$A$_{0.1}$MnO$_3$ (A: Li, Na, K) Nanopowders and Nanoceramics. *Materials* **2020**, *13*, 1788. [CrossRef]

25. Ekambaram, S.; Patil, K.C.; Maaza, M. Synthesis of lamp phosphors: Facile combustion approach. *J. Alloy. Compd.* **2005**, *393*, 81–92. [CrossRef]

26. Fedyk, R.; Hreniak, D.; Łojkowski, W.; Stręk, W.; Matysiak, H.; Grzanka, E.; Gierlotka, S.; Mazur, P. Method of preparation and structural properties of transparent YAG nanoceramics. *Opt. Mater.* **2007**, *29*, 1252–1257. [CrossRef]

27. Degen, T.; Sadki, M.; Bron, E.; König, U.; Nénert, G. The high score suite. In *Powder Diffraction*; Cambridge University Press: Cambridge, UK, 2014; Volume 29, pp. S13–S18.

28. Van Roosmalen, J.A.M.; Cordfunke, E.H.P.; Helmholdt, R.B.; Zandbergen, H.W. The defect chemistry of lamno3±δ. 2. structural aspects of lamno3+δ. *J. Solid State Chem.* **1994**, *110*, 100–105. [CrossRef]

29. Ma, F.; Jiao, Y.; Jiang, Z.; Du, A. Rhombohedral Lanthanum Manganite: A New Class of Dirac Half-Metal with Promising Potential in Spintronics. *ACS Appl. Mater. Interfaces* **2018**, *10*, 36088–36093. [CrossRef]

30. Markovich, V.; Fita, I.; Mogilyansky, D.; Wisniewski, A.; Puzniak, R.; Titelman, L.; Vradman, L.; Herskowitz, M.; Gorodetsky, G. Effect of particle size on magnetic properties of $LaMnO_3 + \delta$ nanoparticles. *Superlattices Microstruct.* **2008**, *44*, 476–482. [CrossRef]

31. Handbook on the Physics and Chemistry of Rare Earths, Volume 33—1st Edition. Available online: https://www.elsevier.com/books/handbook-on-the-physics-and-chemistry-of-rare-earths/gschneidner/978-0-444-51323-6 (accessed on 20 November 2020).

32. Gluchowski, P.; Stręk, W. Luminescence and excitation spectra of $Cr^{3+}:MgAl_2O_4$ nanoceramics. *Mater. Chem. Phys.* **2013**, *140*, 222–227. [CrossRef]

33. Zhao, Y.; Zhang, J. Microstrain and grain-size analysis from diffraction peak width and graphical derivation of high-pressure thermomechanics. *J. Appl. Crystallogr.* **2008**, *41*, 1095–1108. [CrossRef]

34. Gálvez, M.E.; Jacot, R.; Scheffe, J.; Cooper, T.; Patzke, G.; Steinfeld, A. Physico-chemical changes in Ca, Sr and Al-doped La–Mn–O perovskites upon thermochemical splitting of CO_2 via redox cycling. *Phys. Chem. Chem. Phys.* **2015**, *17*, 6629. [CrossRef] [PubMed]

35. Mikhaylov, V.I.; Zubov, E.E.; Pashchenko, A.V.; Varyukhin, V.N.; Shtaba, V.A.; Dyakonov, V.P.; Szewczyk, A.; Abal'oshev, A.; Piotrowski, K.; Lewandowski, S.J.; et al. Comparison of pressure, magnetic-field, and excess manganese effects on transport properties of film and bulk ceramic La–Ca manganites. *Low Temp. Phys.* **2006**, *32*, 139–147. [CrossRef]

36. Guarieiro, L.L.N.; Guarieiro, A.L.N. Impact of the Biofuels Burning on Particle Emissions from the Vehicular Exhaust. In *Biofuels—Status and Perspective*; InTech: London, UK, 2015.

37. Zhang, C.; Wang, C.; Zhan, W.; Guo, Y.; Guo, Y.; Lu, G.; Baylet, A.; Giroir-Fendler, A. Catalytic oxidation of vinyl chloride emission over $LaMnO_3$ and $LaB_{0.2}Mn_{0.8}O_3$ (B = Co, Ni, Fe) catalysts. *Appl. Catal. B Environ.* **2013**, *129*, 509–516. [CrossRef]

38. Qi, G.; Yang, R.T. Characterization and FTIR studies of $MnOx$-CeO_2 catalyst for low-temperature selective catalytic reduction of NO with NH_3. *J. Phys. Chem. B* **2004**, *108*, 15738–15747. [CrossRef]

39. Wang, F.; Dai, H.; Deng, J.; Bai, G.; Ji, K.; Liu, Y. Manganese Oxides with Rod-, Wire-, Tube-, and Flower-Like Morphologies: Highly Effective Catalysts for the Removal of Toluene. *Environ. Sci. Technol.* **2012**, *46*, 4034–4041. [CrossRef] [PubMed]

40. Kucharczyk, B.; Tylus, W. Partial substitution of lanthanum with silver in the $LaMnO_3$ perovskite: Effect of the modification on the activity of monolithic catalysts in the reactions of methane and carbon oxide oxidation. *Appl. Catal. A: Gen.* **2008**, *335*, 28–36. [CrossRef]

41. Zhou, T.; Fan, W.; Liu, Y.; Wang, X. Comparative assessment of the chronic effects of five nano-perovskites on Daphnia magna: A structure-based toxicity mechanism. *Environ. Sci. Nano* **2018**, *5*, 708–719. [CrossRef]

42. Figueiras, F.G.; Karpinsky, D.; Tavares, P.B.; Gonçalves, J.N.; Yañez-Vilar, S.; Moreira Dos Santos, A.F.; Franz, A.; Tovar, M.; Agostinho Moreira, J.; Amaral, V.S. Novel multiferroic state and ME enhancement by breaking the AFM frustration in $LuMn_{1-x}O_3$. *Phys. Chem. Chem. Phys.* **2017**, *19*, 1335–1341. [CrossRef]

43. Troyanchuk, I.O.; Bushinsky, M.V.; Karpinsky, D.V.; Sikolenko, V.V.; Gavrilov, S.A.; Silibin, M.V.; Franz, A.; Ritter, C. Magnetic and magnetotransport properties of $La_{1-x}Sr_xMn_{0.5}Co_{0.5}O_3$ perovskites. *Ceram. Int.* **2018**, *44*, 1432–1437. [CrossRef]

44. Coey, J.M.D.; Viret, M.; Von Molnár, S. Mixed-valence manganites. *Adv. Phys.* **1999**, *48*, 167–293. [CrossRef]

45. García-Muñoz, J.; Fontcuberta, J.; Martinez, B.; Seffar, A.; Pinol, S.; Obradors, X. Magnetic frustration in mixed valence manganites. *Phys. Rev. B Condens. Matter Mater. Phys.* **1997**, *55*, R668–R671. [CrossRef]

Publisher's Note: MDPI stays neutral with regard to jurisdictional claims in published maps and institutional affiliations.